

Single-Stimulus Functional MRI Produces a Neural Individual Difference Measure for Autism Spectrum Disorder

James T. Lu^{1,2,3}, Kenneth T. Kishida⁴, Josepheen De Asis-Cruz⁵, Terry Lohrenz⁴, Diane Treadwell-Deering⁶, Michael Beauchamp⁷, and P. Read Montague^{1,4,8}

¹Wellcome Trust Centre for Neuroimaging, University College London; ²Human Genome Sequencing Center, Baylor College of Medicine; ³Department of Structural and Computational Biology and Molecular Biophysics, Baylor College of Medicine; ⁴Virginia Tech Carilion Research Institute; ⁵Department of Neuroscience, Baylor College of Medicine; ⁶Menninger Department of Psychiatry and Behavioral Sciences, Baylor College of Medicine; ⁷Department of Neurobiology and Anatomy, University of Texas Health Science Center, Houston; and ⁸Department of Physics, Virginia Tech

Abstract

Functional MRI typically makes inferences about neural substrates of cognitive phenomena at the group level. We report the use of a single-stimulus blood-oxygen-level-dependent (BOLD) response in the cingulate cortex that differentiates individual children with autism spectrum disorder from matched typically developing control children with sensitivity and specificity of 63.6% and 73.7%, respectively. The approach consists of passive viewing of self and other faces from which an individual difference measure is derived from the BOLD response to the first self-face image only. The method, penalized logistic regression, requires no averaging over stimulus presentations or individuals. These findings show that single-stimulus functional MRI responses can be extracted from individual subjects and used profitably as a neural individual difference measure. The results suggest that single-stimulus functional MRI can be developed to produce quantitative neural biomarkers for other developmental disorders and may even be useful in the rapid typing of cognition in healthy individuals.

Keywords

autism, cognitive neuroscience, neuropsychology

Received 11/17/13; Revision accepted 8/18/14

Functional MRI (fMRI) has become a major tool in cognitive neuroscience in which blood-oxygen-level-dependent (BOLD) measurements throughout the brain are used to identify spatiotemporal neural dynamics associated with variables of interest (Huettel, Song, & McCarthy, 2008). This general approach is carried out almost exclusively in terms of averages of BOLD responses over multiple presentations of stimuli because of relatively low signal-to-noise issues in the raw BOLD signal. Averaging within a single individual is often followed by averaging across individuals to generate group-level summaries about neural responses to stimuli. The presumed need for averaging presents one barrier to using fMRI as a method for generating rapid, individual difference responses useful

for characterizing healthy or diseased cognition. Moreover, the intrinsic sluggishness and spatial imprecision of the BOLD response contributes to the general perception that fMRI is a useful neuroimaging modality only in “averaging mode.” Here, we present new results that suggest that this view is incomplete and that fMRI can be used to generate a single-stimulus measurement useful as an individual difference measure and biomarker

Corresponding Author:

James T. Lu, Human Genome Sequencing Center, Baylor College of Medicine, One Baylor Plaza, MS: BCM226, Houston, TX 77030
E-mail: jtl@bcm.edu

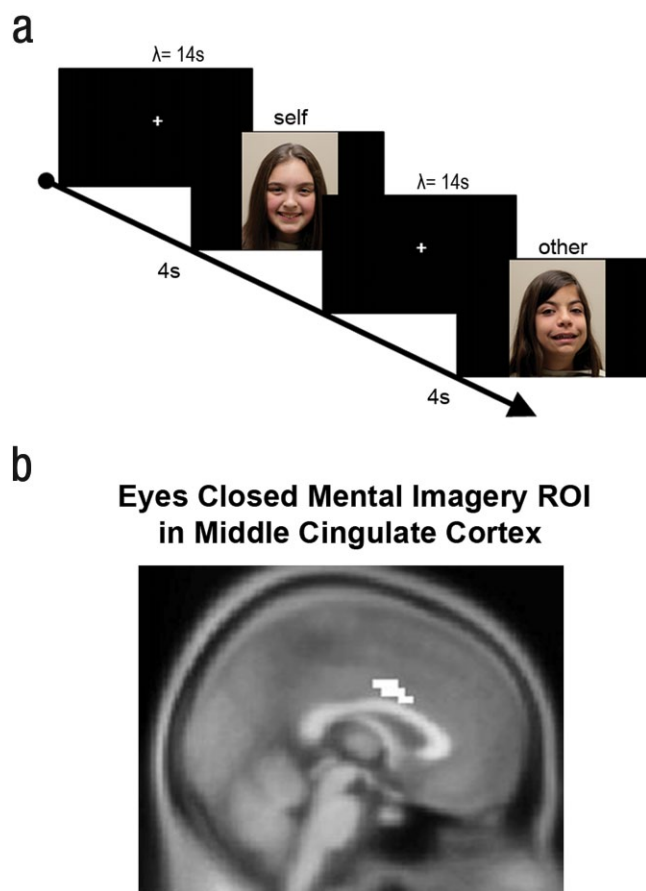


Fig. 1. Example stimulus display and region of interest (ROI). The stimulus display (a) contains a picture of the subject (self) and a picture of a single age-, gender-, and IQ-matched individual (other). Images were shown in random order with Poisson distributed interstimulus intervals ($\lambda = 14$). Demographics are reported in Table S2 in the Supplemental Material. The picture (b) shows independently identified middle cingulate cortex voxels from Kishida, Li, Schwind, and Montague (2012)—specifically, a 10-voxel mask from an eyes-closed mental-imagery task that defined an ROI in adults (Montreal Neurological Institute coordinates).

in one of the most common neurodevelopmental disorders—autism spectrum disorder (ASD).

Our investigation exploring the possibility of using a single-stimulus approach in ASD stems from extensive prior work, which has demonstrated that the middle cingulate cortex (MCC) is particularly responsive during social exchange in a manner that is consistent with the hypothesis that this region is important for cognitive processes related to perspective taking. Specifically, Tomlin et al. (2006) showed that activity in the MCC tracked the active agent (i.e., “me” vs. “not me”) during a social-exchange experiment involving 100 pairs of subjects. Following this work, Chiu et al. (2008) demonstrated that one of these agent-specific responses (the “self-response”) in the MCC was diminished in individuals diagnosed with ASD. Chiu et al. also showed that diminished responses

in the MCC were positively correlated with symptom severity in the ASD cohort. In the same report, Chiu et al. performed a visual-imagery experiment with a sample of 81 accomplished athletes and 27 healthy adults. Using an eyes-closed mental-imagery task, Chiu et al. showed that the same pattern of activity (i.e., self-response along the MCC) could be elicited during eyes-closed mental imagery of first-person perspective taking but not during third-person perspective taking. Kishida, Li, Schwind, and Montague (2012) hypothesized that the region of the MCC that was engaged during perspective taking (and social exchange) and was diminished in the ASD cohort could be specifically activated by showing subjects pictures of themselves. Using a passive-picture-viewing task in healthy adults and the region of interest (ROI) defined in the eyes-closed mental-imagery task, Kishida et al. showed that, indeed, the MCC differentiated pictures of “self faces” from pictures of “other faces.”

Taken together, these results suggested the hypothesis that a similar picture-viewing assay might elicit signals in this same ROI strong enough to produce a neural measure that might also differentiate children diagnosed with ASD from age-matched typically developing (TD) children (cohort-level statistics are provided in Table S2 in the Supplemental Material available online). We also included adult controls to evaluate consistency with past findings. We designed a full-length passive-picture-viewing paradigm to test this hypothesis; however, two empirical findings suggested the necessity of exploring a reduced experimental design. First, the duration of the full-length experiment (approximately 12 min) proved too long for children diagnosed with ASD to remain still in the fMRI scanning environment. Second, in both ASD and TD children, an effect consistent with repetition suppression of BOLD responses in the MCC to repeated presentations of both self and other images suggested that an “average brain response” to multiple presentations was very different from responses to a more reduced design. Following these results, we tested the most extreme version of a “reduced experimental design” and demonstrated that a machine-learning approach and single-stimulus fMRI data from an a priori-prescribed ROI can produce results consistent with a rapidly assessable individual difference measure for ASD.

Method

Stimuli

Photographs of each subject were taken prior to scanning. Subjects were draped around the shoulders to ensure image uniformity. They were instructed to gaze directly at the camera while assuming different head angles. Head angle was varied to reduce habituation to

repeated presentations of face images. In the scanner, subjects were shown 15 pictures of themselves (self face) and 15 unique pictures of an age- and gender-matched individual (other face; see Fig. 1a for example stimulus display). A computer-controlled projector was used to generate the images that were displayed to subjects using an overhead mirror mounted on the radiofrequency coil. Images were shown for 4 s in random order with random interstimulus intervals drawn from a Poisson distribution with parameter value (λ) equal to 14 s. Thus, the starting image for each subject was randomized. Subjects were instructed to focus on the faces or on the white fixation cross (displayed during the interstimulus window). Only TD subjects were used as other (i.e., control) images.

Subjects

We recruited 39 adults with no known neuropsychiatric disorders, 51 TD children, and 35 children with ASD (see Table S2 in the Supplemental Material) from the Houston metropolitan area by word of mouth and advertisements. In addition, subjects with ASD were also referred from the Texas Children's Hospital's Autism Center. After initial assessment using basic fMRI exclusion criteria, we invited the remaining qualified children (TD children: $n = 45$; ASD children: $n = 27$) to Baylor College of Medicine for familiarization with the scanning environment, scanning, and assessments. Autism Diagnostic Observation Schedule (ADOS) scores were available for 20 of the 27 children with ASD (Lord, Rutter, DiLavore, & Risi, 2001). In 12 of these 20 subjects, the diagnoses were reconfirmed by the Autism Diagnostic Interview-Revised (ADI-R; Le Couteur, Lord, & Rutter, 2003). The remaining 7 of these 27 patients were evaluated in autism centers at tertiary hospitals and diagnosed on the basis of clinical presentation and developmental history. Last, scores from the Social Responsiveness Scale (Constantino & Todd, 2003) and the second edition of the Kaufman Brief Intelligence Test (Kaufman & Kaufman, 2004) were obtained for a subset of ASD and TD subjects (see Table S2 in the Supplemental Material). The institutional review board at Baylor College of Medicine approved the study protocol. Parents signed informed written consent and children provided assent.

Image acquisition

Imaging was performed using a 3-T Siemens Allegra head-only scanner and 3-T Siemens Trio full-body scanner; 39 of the 45 TD children and 26 of the 27 ASD children were scanned in the Trio scanner. An analysis of peak differences between and within ASD and TD populations showed that no differences in hemodynamic responses were found to be attributable to the employed scanner. A localizer image was acquired first followed by

high-resolution T1-weighted structural images (192 slices; in-plane resolution: 256×256 ; field of view: 245 mm; slice thickness: 1 mm). Continuous whole-brain imaging was then performed as subjects viewed self and other faces on the screen. Regional brain activation was measured using changes in BOLD fMRI signal. The parameters for the functional sequence are as follows: echo-planar imaging, gradient recalled echo; repetition time = 2,000 ms; echo time = 30 ms; flip angle = 90; 64×64 matrix (in-plane resolution); 34 (4-mm) axial slices positioned 30° to the anterior commissure/posterior commissure line.

Data were preprocessed and analyzed using the SPM8 software package (see <http://www.fil.ion.ucl.ac.uk/spm/software/spm8/>; Friston, Penny, Ashburner, Kiebel, & Nichols, 2006). During preprocessing, functional brain images were temporally realigned using linear interpolation to correct for variability in the timing of slice acquisition, spatially realigned using a 6-parameter rigid-body transformation to correct for head movements, and coregistered onto high-resolution/high-contrast structural images. In adults, images are typically spatially normalized to a Montreal Neurological Institute template (SPM's echo-planar imaging template) by applying a 12-parameter affine transformation to facilitate intersubject comparison.

For the children in our study, we generated customized T1-template and tissue-probability maps (i.e., gray matter, white matter, and cerebrospinal fluid priors) using the SPM8 toolbox Template-O-Matic (see <https://irc.cchmc.org/software/tom.php>). This toolbox is based on data obtained from 404 children as part of the normal-brain-development study of the National Institutes of Health (Wilke, Holland, Altaye, & Gaser, 2008). The toolbox takes in the ages and gender of the sample population as input and automatically generates reference images based on parameters obtained from the National Institutes of Health cohort. Children's images were then segmented and normalized using the unified-segmentation model. During normalization, bounding-box parameters of structural and functional images were matched to the adult masks to ensure that image dimensions and origin were the same. Normalized images, in all cohorts, were then spatially smoothed using an 8-mm Gaussian kernel and temporally filtered (cutoff period of 128 s).

ROI analysis

ROI analysis was performed using independently identified MCC voxels from Kishida et al. (2012; see Fig. 1b). This MCC ROI, which was generated from adult patients, was resliced to our custom children's template using nearest-neighbor interpolation. Axial, coronal, and sagittal cuts of the ROI overlaid on the standard adult template and on our child templates generated with the Template-O-Matic toolbox are shown in Figure S8 in the

Supplemental Material. Raw time courses for this ROI were extracted using SPM functions, detrended, and then averaged. Time series were captured for the period from 6 s prior to stimulus presentation to 16 s after stimulus presentation, including the 4-s presentation interval. Data in this period were linearly interpolated (using MATLAB function `interp.m`). Time series were captured for the first presentation of the self and other images for each individual. BOLD responses were presented as percentage signal change from baseline BOLD rates (−6 s to 0 s, where $t = 0$ is the stimulus presentation). The peak activation was defined as the mean response 6 s to 8 s after stimulus presentation relative to the response measured just prior to the stimulus onset (−6 s to 0 s).

Subject inclusion criteria

One adult of 39 was excluded from analysis because of technical problems during image acquisition (adults: $n = 38$; 14 males, 24 females; mean age = 29.9 years, ± 9.5). Of the 51 TD children originally recruited, 6 were initially excluded from analysis: 2 because of technical problems during scanning; 1 as a result of the subject's decision to discontinue with the study; 1 because the subject fell asleep during the task; and 3 because of excessive head movement (more than 3.5 mm), resulting in 45 TD subjects. Out of the 35 subjects with ASD, 8 were initially excluded (27 remaining) from the analysis: 1 because of atypical brain morphology; 5 because of excessive head movement (exclusion criteria was instantaneous head motions greater than ± 3.5 mm during the first presentations of self and other pictures (6 s pre-stimulus and 16 s post-stimulus); and 2 as a result of technical issues related to scanning that prevented recording of these subjects' brain responses to the first stimulus presentation.

For the ROI analysis, a second inclusion criterion was used to remove hypervariable hemodynamic responses to ensure data quality. Subjects with high MCC signal variability on the first presentation of the self or other image were excluded from analysis to ensure that outlier values did not dominate the BOLD response and confound the results. Removal of BOLD responses that may be contaminated with noise can be especially important when looking at a single-stimulus response.

Signal variability was measured as the standard deviation of the BOLD time course from 6 s prior to presentation to 16 s postpresentation. Outliers for signal variability were defined as having a standard deviation greater than median (of population) plus or minus 3 times the inner quartile range for all hemodynamic responses (see Fig. S9 and Table S3 in the Supplemental Material). Given that signal variations in ASD and TD children were not statistically different (data not shown), these data were

combined and analyzed as a single "child" population. Subjects with MCC signal standard deviation of more than 0.80% for TD and ASD subjects and 0.53% for adults were removed from our single-stimulus ROI analysis. Thus, 33 of 38 adults, 38 of 45 TD children, and 22 of 27 ASD children were retained for our ROI analysis. Individuals excluded from analysis did not have single-stimulus hemodynamic trajectories that resemble typical BOLD responses (see Fig. S10 in the Supplemental Material). In fact, many appeared to have large negative inflections or a sinusoidal pattern. Incidentally, all individuals who were excluded for variable self-face responses were also independently excluded for high-variability other-face responses. This finding further reinforced the hypothesis that the variability in these BOLD trajectories were due to a common factor, such as head movement (Power, Barnes, Snyder, Schlaggar, & Petersen, 2012), or some other unknown factor.

Classifier development for penalized regression model

Penalized regressions were computed using the `glmnet` package (R 2.15.1; Friedman, Hastie, Höfling, & Tibshirani, 2007; Friedman, Hastie, & Tibshirani, 2010; Tibshirani, 1996). Receiver operating characteristic (ROC) curves were plotted on MATLAB 2012b using the `perfcurve` function. Before computing parameter values, we first reweighted the value of individual samples such that the optimization used "equal-sized" populations. Given our sample numbers of 38 TD children and 22 ASD children, this was akin to increasing the value of each ASD sample by 1.72 (38/22). By reweighting the samples, we improved sensitivity and specificity of the classifier for the minor population (Cramer, 2013).

Penalized regression is a variable selection technique that shrinks some coefficients and sets others to 0. The least absolute shrinkage and selection operator, or *lasso* function, is a variable selection technique that utilizes an L^1 -norm penalty. The L^1 -norm penalty alters the standard cross-entropy loss objective function (see the Methods section in the Supplemental Material) to the following:

$$E(w) = - \sum_{n=1}^N \{y_n \ln \sigma(X\beta) + (1 - y_n) \ln(1 - \sigma(X\beta))\} - \lambda \sum_{k=1}^p |\beta_k|$$

where λ is a nonnegative regularization parameter or amount of penalization. Akin to choosing the number of predictors in a regression model, lambda is changed to

increase or decrease the number of nonzero components. Larger values of lambda result in more beta coefficients being set to 0. The value of lambda that minimizes misclassification error can be computed using K-fold cross-validation (Friedman et al., 2007; see Fig. S11 in the Supplemental Material).

Cross-validation. Cross-validation for different levels of penalization also allows one to visualize how models with different amounts of covariates perform on independent data sets. In K-fold cross-validation (Bishop, 2006), the data are partitioned into K subsets. For K repeats, one subset is selected as the “validation set,” and the remaining $K - 1$ subsets are iteratively used to train the model and tested against the validation set. The test statistic, misclassification error or deviance, is computed for each repeat and then averaged to provide a single estimate. Using cross-validation, one can determine lambda such that the desired statistic is optimized. Cross-validation is included in the glmnet computational package; lambda is selected using the “1se” heuristic. This heuristic favors a more parsimonious model in which the expected error is within 1 *SE* cross-validation error (Friedman et al., 2010) of the minimal error.

Computation of coefficients. Computation of coefficients in the lasso in the glmnet package is completed using coordinate descent (Friedman et al., 2007; Friedman et al., 2010). Parameter estimation and cross-validation is automated as part of the glmnet package (Friedman, Hastie, & Tibshirani, n.d.).

Results

In a passive-viewing paradigm, adults, TD children, and children diagnosed with ASD were shown 15 presentations each of images of themselves (self) and an age- and sex-matched individual (other; see Fig. 1a). These images were presented in a randomized order such that the starting image for each subject occurred by chance. BOLD responses to self- and other-image presentations were then extracted using the eyes-closed mental-imagery ROI in the MCC (see Fig. 1b). Consistent with previous findings by Kishida et al. (2012), results from the present study indicated that adults ($n = 33$) showed greater response to self faces than to other faces with averaging of all presentations and with a single-stimulus response (see Fig. S1 in the Supplemental Material).

In analyzing data for TD and ASD children, we focused on the hemodynamic response to the first presentation of either self or other stimuli for two reasons: repetition suppression and task length. Repetition suppression is the reduction of neural responses to repeated stimuli due to stimulus recognition and learning (Grill-Spector,

Henson, & Martin, 2006; Henson & Rugg, 2003; Segaert, Weber, de Lange, Petersson, & Hagoort, 2013). In our experimental paradigm, repetition suppression of the BOLD signal was evident by the second image presentation (see Fig. S1 in the Supplemental Material). We found that for all subjects, cohort-level differences in peak hemodynamic response for self and other images were maximal after the first stimulus presentation and did not improve with multiple presentations (data not shown for adult cohort; for data on TD and ASD cohorts, see Figs. S2a and S2b, respectively, in the Supplemental Material).

In addition, we found that longer experimental paradigms reduced the cohort of individuals that were available for analysis. Using an instantaneous movement threshold of plus or minus 3.5 mm, we plotted a Kaplan Meier curve for experimental completion for all participating subjects (see Fig. S3 in the Supplemental Material) by total scanning time. Our task was approximately 12 min in total length. Unlike adult and TD subjects, who were able to voluntarily lie still for extended periods, ASD children showed significant head movement. After 5 min of scanning time, more than 40% of the data from the ASD population could not be analyzed as a result of excessive head movement. However, by reducing scanning time to less than 2 min (i.e., single-stimulus responses), we could retain data from more than 75% of the subjects with ASD.

The challenges associated with full-length experiments in children diagnosed with ASD motivated the exploration of a reduced experimental design; in the extreme, eliciting a reliable brain response to a single stimulus would provide dramatically increased flexibility in the kinds of fMRI experiments that could be designed. Figure 2a and 2b and Figure S3 in the Supplemental Material show the cohort-level hemodynamic response to the first presentation of a self-face image displayed alongside the analogous time series for the first presentation of the other-face image for TD children ($n = 38$; Fig. 2a), ASD children ($n = 22$; Fig. 2b), and adult subjects ($n = 33$; Fig. S3). These data show two clear features at the cohort level. First, single-stimulus responses elicit a large BOLD response in the MCC. In the TD cohort, the peak hemodynamic response differentiates between self-face versus other-face images ($p = .04$, right-sided *t* test; see Fig. 2a and 2c); this result is consistent with analyses of adults in the present study ($p = .03$, right-sided *t* test; see Fig. S3) and previously reported findings in adults (Kishida et al., 2012). Second, unlike TD children, single-stimulus peak BOLD responses in the ASD cohort did not differentiate self from other images ($p = .16$, right-sided *t* test). When we compared the TD and ASD cohorts, results showed that peak responses to self-face images differentiated the TD and ASD cohorts ($p = .04$, right-sided *t* test), but responses to other-face images did not ($p = .22$, right-sided

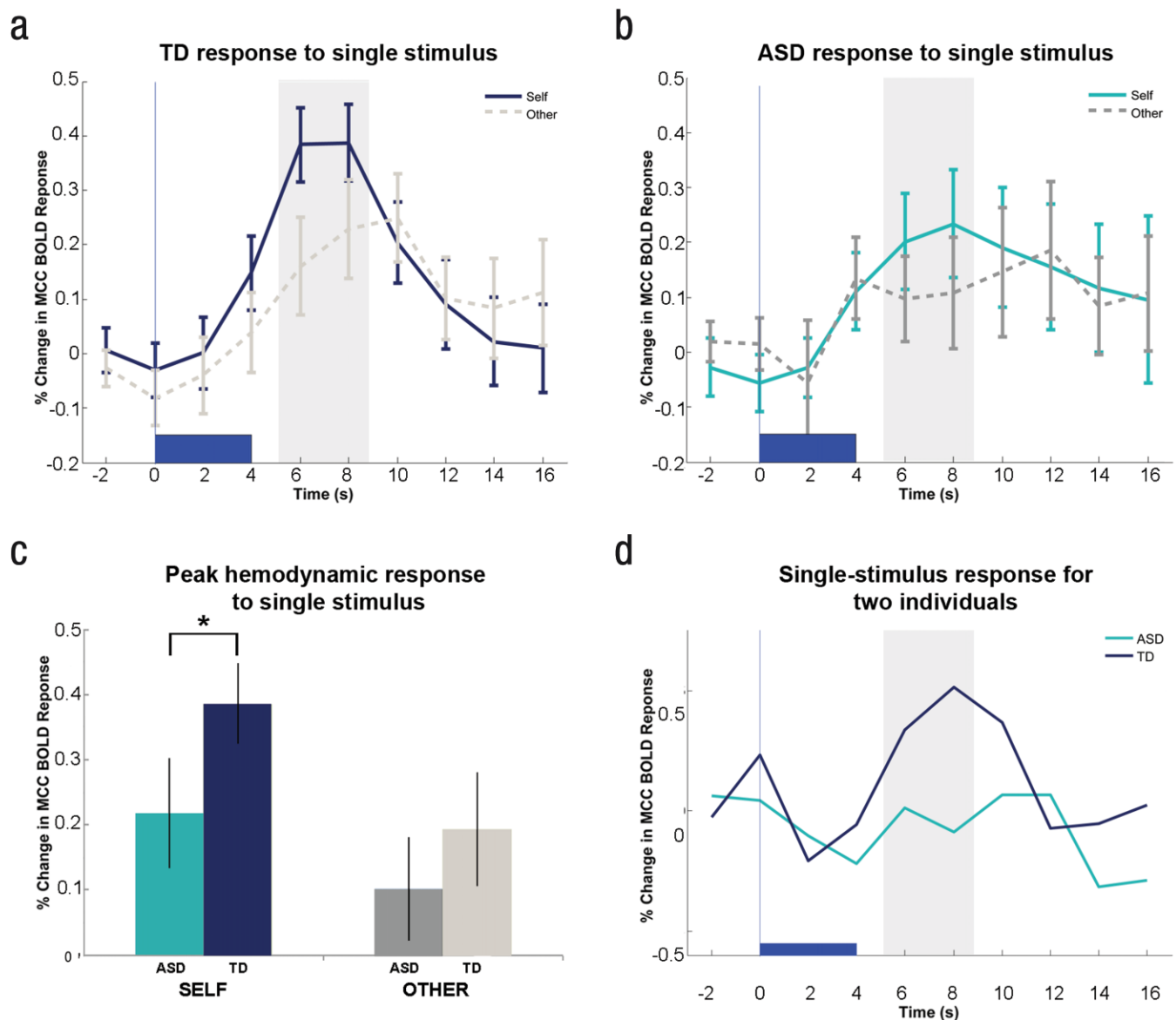


Fig. 2. Results: single-stimulus responses. The graphs show (a) time series for single-stimulus presentation averaged over TD children ($n = 38$), (b) time series for single-stimulus presentation averaged over ASD children ($n = 22$), (c) peak hemodynamic response for ASD and TD children for single-stimulus self and other images (asterisk indicates $p < .05$), and (d) hemodynamic responses to single-stimulus self-face images for single ASD and TD individuals. Trajectories for all subjects are shown in Figure S2 in the Supplemental Material. MCC = middle cingulate cortex; BOLD = blood-oxygen-level-dependent; TD = typically developing; ASD = autism spectrum disorder. Error bars represent the standard error.

t test). Thus, differences across the two populations arose specifically for the time-series responses for the self-face picture (see Fig. 2c).

To test whether TD and ASD subjects were actively viewing the face-image stimuli, we extracted responses from bilateral fusiform face area (FFA) in 21 control adults in a separate task using a passive-viewing paradigm of faces and objects (see Fig. S5 in the Supplemental Material; Kanwisher & Yovel, 2006). Using a general linear model contrast, we assessed visual responses in the fusiform gyrus with particular attention paid to the FFA to

determine whether subjects viewed the images. We found that the bilateral FFA activated robustly in both cohorts in response to self and other face images. Although some studies have reported decreased FFA activity in ASD patients (Deeley et al., 2007; Humphreys, Hasson, Avidan, Minshew, & Behrmann, 2008), other studies have shown that familiarity (Pierce, Haist, Sedaghat, & Courchesne, 2004), age (Pierce & Redcay, 2008), and attention (Hadjikhani et al., 2004) engage the FFA in autism. The lack of differences in FFA activation between TD and ASD children (see Fig. S5 in the Supplemental Material)

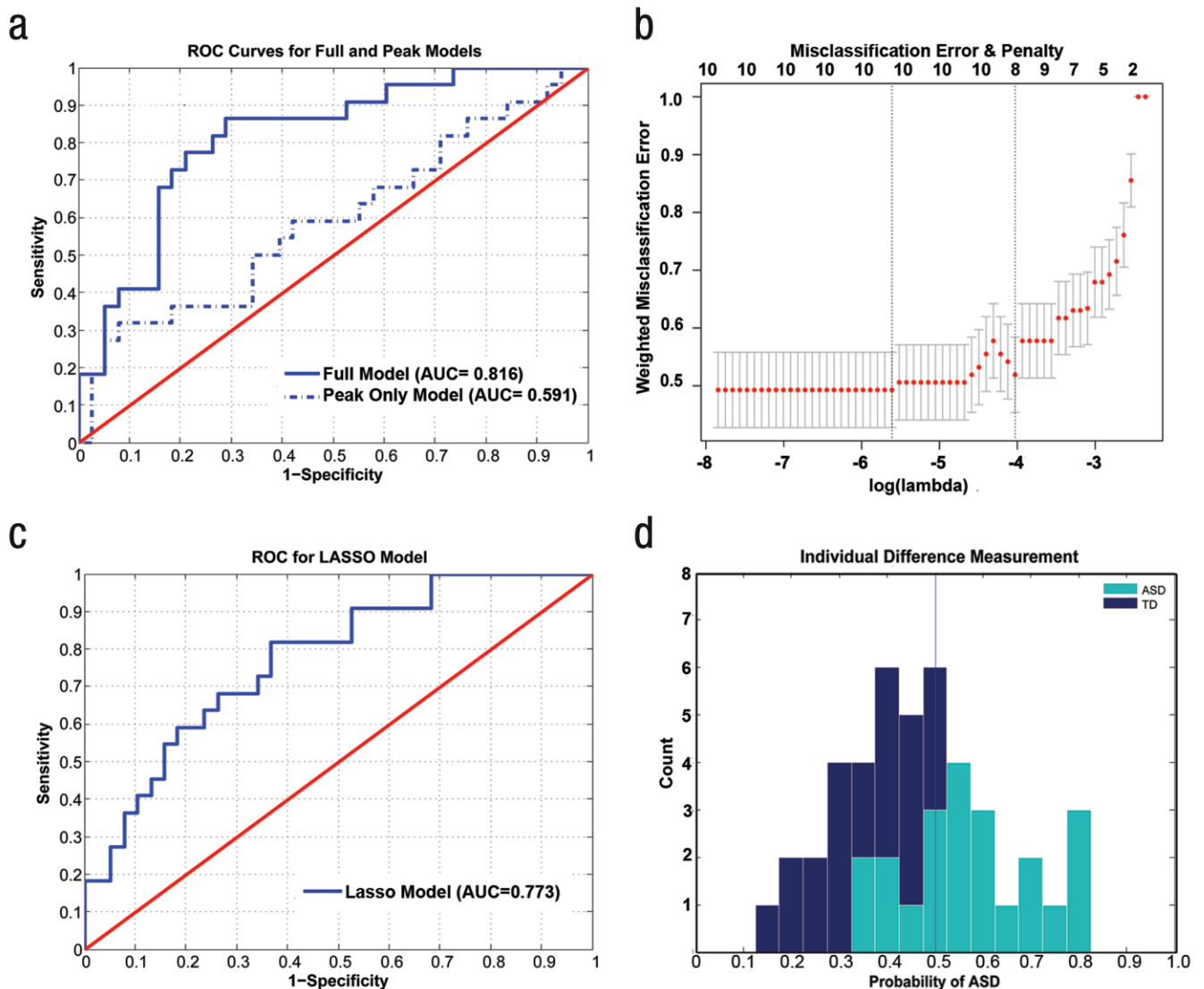


Fig. 3. Differences in blood-oxygen-level-dependent middle cingulate cortex responses to single-stimulus self-face images classifies individual subjects. The graph in (a) shows ROC curves for a full logistic model and a model based on averaging peak responses. The graph in (b) shows misclassification error versus penalization in a penalized logistic regression model. Lambda is the amount of penalization. The top of the graph shows the number of variables (i.e., degrees of freedom) included in the model as penalization changes. Less penalization, $\log(\lambda)$, results in more degrees of freedom. Two vertical lines are plotted: The left line is the penalization that produced minimal misclassification error; the right line is the penalization (“1se”) that is within 1 standard cross-validation error of the minimum error. Lambda is selected using the 1se rule, given that the error is statistically equivalent, but the model is more parsimonious. Error bars represent the standard error. The graph in (c) shows ROC curves for a penalized logistic regression model using a leave-one-out cross-validation. The penalized cross-validated model uses data from only eight covariates. The graph in (d) shows histograms of individual difference measurements, $p(\text{status} = \text{ASD} \mid M)$, given the penalized model (M). The D' between the ASD and TD cohorts is 1.50 for the single-shot measurements and 1.61 for the full model. ROC = receiver operating characteristic; AUC = area under the curve; ASD = autism spectrum disorder; TD = typically developing.

during image presentations suggests that both cohorts' brains detected the face images throughout the task ($p_{\text{unc}} < .005$, $k = 10$; Pessoa, McKenna, Gutierrez, & Ungerleider, 2002).

Across the ASD and TD cohorts, the hemodynamic-time-series differences to self-face images (Fig. 2a and 2b) provided an opportunity to develop an individual difference measurement, that is, a single parameter value

that summarizes an individual's BOLD-response time series to a single-stimulus self-face image (Fig. 2d and Fig. S4). One simple approach is to discriminate the TD and ASD populations using the peak response. Discriminant classification of disease status based solely on the percentage signal change in the peak activation of the BOLD response resulted in sensitivity and specificity of 54.6% and 57.9%, respectively, and an area under the

Table 1. Comparison of Coefficients for the Full Logistic Regression Model With Coefficients From the Penalized Model

ID	Coefficient	Full model (logit)		Penalized model
		Estimate	Pr(> z)	Estimate
0	Intercept	2.917 (0.937)	0.002	1.487
1	Age	-0.216 (0.069)	0.002	-0.104
2	First-or-not-first	1.102 (0.509)	0.030	0.443
3	-2.00	24,100 (56,430)	0.669	0.000
4	0 (Presentation)	24,100 (56,430)	0.669	0.000
5	2.00	24,100 (56,430)	0.669	0.000
6	4.00	5.327 (1.358)	0.000	1.591
7	6.00	-4.998 (1.393)	0.000	-2.270
8	8.00	-1.729 (1.008)	0.086	-0.226
9	10.00	2.345 (0.916)	0.010	0.362
10	12.00	0.012 (0.979)	0.991	0.000
11	14.00	0.586 (0.726)	0.419	0.474
12	16.00	0.301 (0.536)	0.574	0.122

Note: Standard errors are shown in parentheses. The model is over parameterized; parameters for time since onset (seconds = -2, 0, and 2) cannot be computed with precision.

curve (AUC) of 0.591 (see Table S1, Fig. 3a and Fig. S6 in the Supplemental Material); this is a subpar classification of disease state for individuals. However, we found that we could improve classification by including more data from the time series. Using only data captured by a peak hemodynamic response discards information encoded elsewhere in the dynamics of the ROI response. In addition, the hemodynamic response to any stimulus already includes a profound smoothing effect that is compounded by further averaging. To improve classification, we used the information of an entire time series in the preselected ROI and employed a penalized logistic regression. This classification method generates, for each time-series sample after a self-picture presentation, the probability of being assigned to the ASD group, for example, $p(\text{status} = \text{ASD} \mid M)$, given the model (M).

In ordinary logistic regression, the objective function is the cross-entropy loss (see the Methods section in the Supplemental Material; Bishop, 2006). Although this method is commonly used and results in low bias classification, models that include a large number of covariates often have high variance due to overfitting. Such overparameterized models can have low prediction accuracy for future data sets (Tibshirani, 1996). Accordingly, we used a variable selection technique that employs an L1 penalization, which shrinks some coefficients and sets others to 0. One variation of this method is called lasso. The lasso objective function includes a penalty term (λ), which is a nonnegative regularization parameter (Count, 2010; see the Method section). Akin to choosing the number of predictors in a regression model, lambda is changed to increase or decrease the number of nonzero (p) components. Larger values of lambda result in more

beta coefficients being set to 0. The value of lambda that minimizes misclassification error can be computed using K-fold cross-validation. Penalization created a reduced model that excluded covariates that do not affect the outcome variable. In a practical sense, if a model contains multiple correlated covariates, as we would expect for time-series data, most coefficients will be set to 0 (see the Methods section in the Supplemental Material for more details).

We used age, a “first-or-not-first” covariate that indicates whether the first stimulus was also the starting image, and the time-series data for the BOLD response for the self-face image as 12 covariates in our model. To evaluate classification, we initially performed a logistic regression using a standard general linear model package in R. As expected, the full model is overparameterized because of autocorrelation that results in poorly estimated parameters (see Table 1) and is difficult to interpret. AUC for the ROC curve for this full model was 0.816 (see Fig. 3a). To improve parameter estimation, we employed leave-one-out cross-validation and penalization to identify a model that minimizes misclassification (Friedman et al., 2010). We found that the optimal model reduced the number of covariates from 12 to 8 (see Fig. 3b). AUC for this reduced model was 0.773 (see Fig. 3c), and sensitivity and specificity for this model were 63.6% and 73.7%, respectively (see Table 2). The coefficients emphasize not only the difference in amplitude in self-face responses but also differences in the relaxation and latency of the BOLD response (see Fig. 2a and 2b). An evaluation of misclassification error for different numbers of variables revealed that the penalized model would have similar expected misclassification error on future

Table 2. Two-by-Two Classification for the Cross-Validated Penalized Model

Prediction	Actual		
	ASD children	TD children	Total
ASD children	14	10	24
TD children	8	28	36
Total	22	38	60
Sensitivity (%)	63.64		
Specificity (%)	73.68		

Note: ASD = autism spectrum disorder; TD = typically developing.

data sets as would a full model (see Fig. 3b). The computed individual difference measurements for each individual can be aggregated into separate distributions; D' between the two cohorts was computed to be 1.50 in the reduced model (see Fig. 3d).

To evaluate the specificity of our response to the single-stimulus self-face image, we also repeated the procedure for the first presentation of the other-face image. After applying the same leave-one-out cross-validation and penalization, we found that the generated model did not include any time-series information from the other-face images (coefficients were set to 0; see Fig. S7a in the Supplemental Material). This model included only a constant and the age covariate. It generated a ROC curve with an AUC of 0.607 (see Fig. S7b in the Supplemental Material). These results are consistent with (although not definitive) the specificity of self faces, but not other faces, for eliciting differentiating responses in the MCC across TD and ASD individuals.

Discussion

ASD is a highly heterogeneous (Lichtenstein, Carlström, Råstam, Gillberg, & Anckarsäter, 2010; Schaaf & Zoghbi, 2011) disorder with concomitant diagnostic complexities. Neuroimaging and neuropathology studies have revealed that brain growth and organization are fundamentally different in ASD (Johnson & Myers, 2007); thus, usage of MRI as a biological assay holds great interest as a supplement to current diagnostic techniques. Researchers have used anatomical differences in grey- and white-matter volume (Neeley et al., 2007) and in cortical thickness (Jiao et al., 2010) and whole-brain pattern classification (Ecker et al., 2010) to classify TD and ASD children. Like many of these previous proof-of-concept studies on alternative assays to diagnose ASD, our study is not powered to evaluate test-and-retest reliability.

Prior fMRI work has relied primarily on averaging over multiple presentations to determine group-level responses to stimuli. To our knowledge, this is the first fMRI experiment to exploit a single-stimulus-induced BOLD time

series that also produced a neural individual difference measure. Our successful elicitation of a single-stimulus result in part relies heavily on our prior work that defined the ROI, the cognitive variable, and their relationship to the population of interest. We present evidence of repetition suppression in our ROI, which begins to occur by the second presentation. The literature (Henson & Rugg, 2003) and our data suggest that it is not yet clear how the meaning of a stimulus changes with repeated presentations within a subject's experimental trial. At a minimum, these results raise unanswered questions about how the cognitive interpretation of a stimulus changes over repeated presentations and how brain responses change respectively. Future work is needed to further explore the difference between single- and multiple-presentation paradigms.

Although our measurement provided only moderate discrimination, we in fact expected that a proportion of ASD and TD samples would be misclassified. First, hemodynamic responses to stimuli vary across the population, and our study numbers are not powered to properly map this variation. Second, the MCC has been linked to perspective taking in individuals (Lombardo et al., 2010), an ability that matures with age (Mitchell & O'Keefe, 2008; Sally & Hill, 2006). One plausible interpretation is that the conflation of disease status and cognitive maturation hampered our ability to discriminate between ASD and TD individuals. Third, although our measurement may map loosely onto *Diagnostic and Statistical Manual of Mental Disorders* (4th ed.; *DSM-IV*; American Psychiatric Association, 1994) clinical criteria for ASD, in particular the axis regarding poor social interaction, these axes leave substantial room for interpretation and have already changed in *DSM-5* (American Psychiatric Association, 2013). Last, given the heterogeneity in ASD presentations (Ronald et al., 2006), we suspect that the most relevant finding in this single-stimulus experiment may be the relatively low misclassification rate of putatively TD children.

In several studies, researchers have explored the sensitivity and specificity of well-known ASD surveys (ADOS and ADI-R) and diagnosis of ASD in comparison with "gold-standard" clinical assessment (Gray, Tonge, & Sweeney, 2008; Ventola et al., 2006). In these studies, patients suspected (by survey) of ASD have yielded sensitivity of and specificity of 0.88 to 0.99 and 0.67 to 0.82 (ADOS) and 0.53 to 0.77 and 0.61 to 0.70 (ADI-R), respectively. Although our results appear comparable at first glance, they may be skewed favorably by selection and model bias. Namely, our enrolled subjects were already diagnosed with ASD by gold-standard clinical assessment, whereas evaluations of ADOS/ADI-R are conducted on suspected patients with blinded physicians. Proper external validation of this paradigm and

model will require a large subject pool recruited using a screening tool, blinding of the evaluating physicians, and model validation using an external cohort, not just internal cross-validation.

The clinical adoption of an MRI biomarker for psychopathology will require, at a minimum, reliable and accurate classification of disease. Furthermore, the success of any potential clinical diagnostic strategy depends on operational reliability—reliability that often derives from simple and cost-effective procedures. Although the simplicity and brevity of single-stimulus paradigms should reduce operator variability, this question has not been adequately explored. Our work suggests that single-stimulus methodologies, in an MCC ROI that was previously identified in several hundred normal individuals in self and other tasks (Chiu et al., 2008; King-Casas et al., 2005; Kishida, King-Casas, & Montague, 2011; Tomlin et al., 2006), may provide accurate classification of disease in ASD patients. Moreover, BOLD time-series data from simple and short paradigms, which had previously been thought to be highly smoothed and noise ridden, may nonetheless provide useful diagnostic information. We are cautiously optimistic that this work may provide a small step toward developing MRI-based applications for screening of psychopathology or other cognitive phenotypes.

Author Contributions

J. T. Lu analyzed the data and drafted the manuscript. K. Kishida planned the experiment and assisted with data analysis. J. De Asis-Cruz performed the experiments and analyzed the data. T. Lohrenz, D. Treadwell-Deering, and M. Beauchamp supervised the experiment and assisted with data analysis. P. R. Montague assisted with experimental design and data analysis. All authors revised the manuscript and approved the final version of the manuscript for submission.

Acknowledgments

The authors would like to thank the NEMO software development team for their assistance in programming the stimulus-presentation scripts and the Human Neuroimaging Laboratory's technological staff for their assistance with recruitment and scanning. J. T. Lu, K. Kishida, and J. De Asis-Cruz contributed equally to this work.

Declaration of Conflicting Interests

The authors declared that they had no conflicts of interest with respect to their authorship or the publication of this article.

Funding

This work was funded by grants from the Kane Family Foundation, Autism Speaks, and the Charles A. Dana Foundation (to P. R. Montague) and by the National Institutes of Health (Grants RO1 DA11723 and RO1 MH085496 to P. R. Montague, Grant T32 NS43124 to K. Kishida, and Grant NRSA F30 MH098571-01 to J. T. Lu).

Supplemental Material

Additional supporting information may be found at <http://cpx.sagepub.com/content/by/supplemental-data>

References

- American Psychiatric Association. (1994). *Diagnostic and statistical manual of mental disorders* (4th ed.). Washington, DC: Author.
- American Psychiatric Association. (2013). *Diagnostic and statistical manual of mental disorders* (5th ed.). Arlington, VA: American Psychiatric Publishing.
- Bishop, C. M. (2006). *Pattern recognition and machine learning*. New York, NY: Springer Science + Business Media.
- Chiu, P. H., Kayali, M. A., Kishida, K. T., Tomlin, D., Klinger, L. G., Klinger, M. R., & Montague, P. R. (2008). Self responses along cingulate cortex reveal quantitative neural phenotype for high-functioning autism. *Neuron*, *57*, 463–473. doi:10.1016/j.neuron.2007.12.020
- Constantino, J. N., & Todd, R. D. (2003). Autistic traits in the general population: A twin study. *Archives of General Psychiatry*, *60*, 524–530. doi:10.1001/archpsyc.60.5.524
- Cramer, J. S. (2013). Predictive performance of the binary logit model in unbalanced samples. *Journal the Royal Statistical Society: Series D (The Statistician)*, *48*, 85–94.
- Deeley, Q., Daly, E. M., Surguladze, S., Page, L., Toal, F., Robertson, D., . . . Murphy, D. G. M. (2007). An event related functional magnetic resonance imaging study of facial emotion processing in Asperger syndrome. *Biological Psychiatry*, *62*, 207–217. doi:10.1016/j.biopsych.2006.09.037
- Ecker, C., Rocha-Rego, V., Johnston, P., Mourao-Miranda, J., Marquand, A., Daly, E. M., . . . Murphy, D. G. (2010). Investigating the predictive value of whole-brain structural MR scans in autism: A pattern classification approach. *NeuroImage*, *49*, 44–56. doi:10.1016/j.neuroimage.2009.08.024
- Friedman, J., Hastie, T., Höfling, H., & Tibshirani, R. (2007). Pathwise coordinate optimization. *Annals of Applied Statistics*, *1*, 302–332. doi:10.1214/07-AOAS131
- Friedman, J., Hastie, T., & Rob, T. (n.d.). Glmnet: Lasso and elastic-net regularized generalized linear models (Version 2013-03-02) [Computer software]. Retrieved from <http://cran.r-project.org/web/packages/glmnet/index.html>
- Friedman, J., Hastie, T., & Tibshirani, R. (2010). Regularization paths for generalized linear models via coordinate descent. *Journal of Statistical Software*, *33*(1), 1–22.
- Friston, K. J., Penny, W. D., Ashburner, J. T., Kiebel, S. J., & Nichols, T. E. (2006). *Statistical parametric mapping: The analysis of functional brain images*. Boston, MA: Academic Press. doi:0123725607
- Gray, K. M., Tonge, B. J., & Sweeney, D. J. (2008). Using the Autism Diagnostic Interview–Revised and the Autism Diagnostic Observation Schedule with young children with developmental delay: Evaluating diagnostic validity. *Journal of Autism and Developmental Disorders*, *38*, 657–667. doi:10.1007/s10803-007-0432-y
- Grill-Spector, K., Henson, R., & Martin, A. (2006). Repetition and the brain: Neural models of stimulus-specific effects. *Trends in Cognitive Sciences*, *10*, 14–23. doi:10.1016/j.tics.2005.11.006

- Hadjikhani, N., Joseph, R. M., Snyder, J., Chabris, C. F., Clark, J., Steele, S., . . . Tager-Flusberg, H. (2004). Activation of the fusiform gyrus when individuals with autism spectrum disorder view faces. *NeuroImage*, *22*, 1141–1150. doi:10.1016/j.neuroimage.2004.03.025
- Henson, R. N. A., & Rugg, M. D. (2003). Neural response suppression, haemodynamic repetition effects, and behavioural priming. *Neuropsychologia*, *41*, 263–270.
- Huettel, S. A., Song, A. W., & McCarthy, G. (2008). *Functional magnetic resonance imaging* (2nd ed.). Sunderland, MA: Sinauer Associates.
- Humphreys, K., Hasson, U., Avidan, G., Minshew, N., & Behrmann, M. (2008). Cortical patterns of category-selective activation for faces, places and objects in adults with autism. *Autism Research*, *1*, 52–63. doi:10.1002/aur.1
- Jiao, Y., Chen, R., Ke, X., Chu, K., Lu, Z., & Herskovits, E. H. (2010). Predictive models of autism spectrum disorder based on brain regional cortical thickness. *NeuroImage*, *50*, 589–599. doi:10.1016/j.neuroimage.2009.12.047
- Johnson, C. P., & Myers, S. M. (2007). Identification and evaluation of children with autism spectrum disorders. *Pediatrics*, *120*, 1183–1215. doi:10.1542/peds.2007-2361
- Kanwisher, N., & Yovel, G. (2006). The fusiform face area: A cortical region specialized for the perception of faces. *Philosophical Transactions of the Royal Society B: Biological Sciences*, *361*, 2109–2128. doi:10.1098/rstb.2006.1934
- Kaufman, A. S., & Kaufman, N. L. (2004). *K-BIT: Kaufman Brief Intelligence Test* (2nd ed.). Circle Pines, MN: American Guidance Service.
- King-Casas, B., Tomlin, D., Anen, C., Camerer, C. F., Quartz, S. R., & Montague, P. R. (2005). Getting to know you: Reputation and trust in a two-person economic exchange. *Science*, *308*, 78–83. doi:10.1126/science.1108062
- Kishida, K. T., King-Casas, B., & Montague, P. R. (2011). Neuroeconomic approaches to mental disorders. *Neuron*, *67*, 543–554. doi:10.1016/j.neuron.2010.07.021
- Kishida, K. T., Li, J., Schwind, J., & Montague, P. R. (2012). New approaches to investigating social gestures in autism spectrum disorder. *Journal of Neurodevelopmental Disorders*, *4*, 14. Retrieved from <http://www.jneurodevdisorders.com/content/4/1/14>
- Le Couteur, A., Lord, C., & Rutter, M. (2003). *The Autism Diagnostic Interview-Revised (ADI-R)*. Los Angeles, CA: Western Psychological Services.
- Lichtenstein, P., Carlström, E., Råstam, M., Gillberg, C., & Anckarsäter, H. (2010). The genetics of autism spectrum disorders and related neuropsychiatric disorders in childhood. *American Journal of Psychiatry*, *167*, 1357–1363. doi:10.1176/appi.ajp.2010.10020223
- Lombardo, M. V., Chakrabarti, B., Bullmore, E. T., Sadek, S. A., Pasco, G., Wheelwright, S. J., . . . Baron-Cohen, S. (2010). Atypical neural self-representation in autism. *Brain*, *133*, 611–624. doi:10.1093/brain/awp306
- Lord, C., Rutter, M., DiLavore, P. D., & Risi, S. (2001). *Autism Diagnostic Observation Schedule*. Los Angeles, CA: Western Psychological Services.
- Mitchell, P., & O'Keefe, K. (2008). Brief report: Do individuals with autism spectrum disorder think they know their own minds? *Journal of Autism and Developmental Disorders*, *38*, 1591–1597. doi:10.1007/s10803-007-0530-x
- Neeley, E. S., Bigler, E. D., Krasny, L., Ozonoff, S., McMahon, W., & Lainhart, J. E. (2007). Quantitative temporal lobe differences: Autism distinguished from controls using classification and regression tree analysis. *Brain & Development*, *29*, 389–399. doi:10.1016/j.braindev.2006.11.006
- Pessoa, L., McKenna, M., Gutierrez, E., & Ungerleider, L. G. (2002). Neural processing of emotional faces requires attention. *Proceedings of the National Academy of Sciences, USA*, *99*, 11458–11463. doi:10.1073/pnas.172403899
- Pierce, K., Haist, F., Sedaghat, F., & Courchesne, E. (2004). The brain response to personally familiar faces in autism: Findings of fusiform activity and beyond. *Brain*, *127*, 2703–2716. doi:10.1093/brain/awh289
- Pierce, K., & Redcay, E. (2008). Fusiform function in children with an autism spectrum disorder is a matter of “who.” *Biological Psychiatry*, *64*, 552–560. doi:10.1016/j.biopsych.2008.05.013
- Power, J. D., Barnes, K. A., Snyder, A. Z., Schlaggar, B. L., & Petersen, S. E. (2012). Spurious but systematic correlations in functional connectivity MRI networks arise from subject motion. *NeuroImage*, *59*, 2142–2154. doi:10.1016/j.neuroimage.2011.10.018
- Ronald, A., Happé, F., Bolton, P., Butcher, L. M., Price, T. S., Wheelwright, S., . . . Plomin, R. (2006). Genetic heterogeneity between the three components of the autism spectrum: A twin study. *Journal of the American Academy of Child and Adolescent Psychiatry*, *45*, 691–699. doi:10.1097/01.chi.0000215325.13058.9d
- Sally, D., & Hill, E. (2006). The development of interpersonal strategy: Autism, theory-of-mind, cooperation and fairness. *Journal of Economic Psychology*, *27*, 73–97. doi:10.1016/j.joep.2005.06.015
- Schaaf, C. P., & Zoghbi, H. Y. (2011). Solving the autism puzzle a few pieces at a time. *Neuron*, *70*, 806–808. doi:10.1016/j.neuron.2011.05.025
- Segaert, K., Weber, K., de Lange, F. P., Petersson, K. M., & Hagoort, P. (2013). The suppression of repetition enhancement: A review of fMRI studies. *Neuropsychologia*, *51*, 59–66. doi:10.1016/j.neuropsychologia.2012.11.006
- Tibshirani, R. (1996). Regression shrinkage and selection via lasso. *Journal of the Royal Statistical Society: Series B (Methodological)*, *58*, 267–288.
- Tomlin, D., Kayali, M. A., King-Casas, B., Anen, C., Camerer, C. F., Quartz, S. R., & Montague, P. R. (2006). Agent-specific responses in the cingulate cortex during economic exchanges. *Science*, *312*, 1047–1050. doi:10.1126/science.1125596
- Ventola, P. E., Kleinman, J., Pandey, J., Barton, M., Allen, S., Green, J., . . . Fein, D. (2006). Agreement among four diagnostic instruments for autism spectrum disorders in toddlers. *Journal of Autism and Developmental Disorders*, *36*, 839–847. doi:10.1007/s10803-006-0128-8
- Wilke, M., Holland, S. K., Altaye, M., & Gaser, C. (2008). Template-O-Matic: A toolbox for creating customized pediatric templates. *NeuroImage*, *41*, 903–913. doi:10.1016/j.neuroimage.2008.02.056